Springer

KSME

Journal of Mechanical Science and Technology 24 (5) (2010) 1111~1118
www.springerlink.com/content/1738-494x
DOI 10.1007/s12206-010-0315-6

Study on the general characteristics of the sound radiation of a rectangular plate with different boundary edge conditions †

Ji Woo Yoo*

CAE Technology Team, Vehicle Technology Center, Hyundai-Kia Motors, Jangduk-Dong Hwaseong-Si, 445-706, Korea

(Manuscript Received May 31, 2009; Revised January 16, 2010; Accepted February 13, 2010)

Abstract

Sound radiation is the most important phenomenon when a structure vibrates, which is strongly dependent on boundary conditions and its shape such as aspect ratio. This paper deals with general aspects of sound radiation from this viewpoint. A particular guided and pinned condition being taken into account here, is that the cross-modal terms can average out for all possible point excitation locations. Then, the average radiation efficiency based on the modal radiation efficiency and corresponding radiation power can numerically be obtained. It is shown that the radiation power of the guided plate is governed by the piston mode as well as the critical frequency. Unlike the pinned plate, no clear corner and edge mode regions below the critical frequency may be found for the guided case. Meanwhile, if the plate damping increases the similar tendency that the radiation efficiency increases below the critical frequency is found, as the vibrational level decreases. For the strip with a large aspect ratio, the radiation power is maximised at frequencies where the wavelength is an integer times the short edge length. This can be seen for both the guided and the pinned boundary conditions.

Keywords: Sound radiation; Radiation efficiency; Guided; Pinned; Rectangular plate; Strip; Modal approach; Farfield

1. Introduction

In automotive vehicles, both structure-borne and airborne noise paths are important to secure NVH targets. Air-borne characteristics are usually investigated based on Statistical Energy Analysis (SEA) which does seem successful [1]. Regarding structure-borne noise, sound radiation may be one of the most important characteristics. The dash firewall is a good example where resonant sound transmission occurs. However, this structure-borne noise problem is still under investigation, as it may be difficult to find general characteristics, since various boundary conditions as well as many numbers of modes of a real complicated structure should be considered.

Therefore, previous studies have generally dealt with simple rectangular plates or strips. Berry [2] studied the influence of boundary conditions on sound radiation, when the modal density is low and below critical frequency. For a finite, simply supported, baffled plate, it is well known that the radiation of sound by a given mode, excited below its modal critical frequency, is due to corners and edges of the plate. While the radiation efficiency is almost the same in the free and guided cases for low order modes, for higher modes it is substantially larger in the guided case. Berry also pointed out that the rigid motions may predominantly contribute to the low frequency sound radiation from free or guided plates. This piston motion is sufficient to provide a good estimate of the radiated power from the free or guided plate. It is mentioned that this would also be true above the critical frequency, although the result was not shown. The study concentrated on individual modes and the corresponding radiation efficiencies. A single point force was applied at a certain location.

Maidanik showed that, the radiation resistance of a large panel at frequencies below the critical frequency, with clamped boundaries that generate nearfield effect, would be twice that of the simply supported case [3]. However, this may only be true for very large structures. In addition, Leppington [4] showed that Maidanik overestimated the radiation resistance at coincidence, using the assumption of high modal densities for the plate. In fact, in the studies of Maidanik and Leppington, the radiation characteristics were considered without including cross-modal contribution, which may provide some resulting discrepancies.

Lomas and Hayek [5] showed that the influence of an elastic restraint, against rotation at the edges of a panel, is least significant for the radiation efficiency, which means pinned and clamped conditions show roughly the same radiation effi-

† This paper was recommended for publication in revised form by Associate Editor Yeon June Kang

*Corresponding author. Tel.: +82 31 368 3351
E-mail address: j.w.yoo@hyundai-motor.com

ciency, which is also shown by Berry [1].

Snyder and Tanaka [6] introduced the contribution of the cross-modal coupling to calculate the total acoustic power at low frequency, by using radiation efficiencies. It was shown that the cross mode contributions are only non-zero for pairs of modes that are either both odd or both even, in a given direction. The cross-modal coupling could have a significant impact on the radiated power, even at a resonance frequency [7].

Xie et al. [8] investigated the averaged radiation efficiency of point-excited rectangular plates, including strips with pinned conditions. A modal summation method is used that is based on the farfield sound intensity. By taking an average over all possible forcing positions on the plate, the cross-modal contributions average out to zero. The general radiation characteristics of a pinned plate were investigated.

Patil and Crocker [9] used an optimization of a commercial FE code. Variation of thickness along the plate can be arranged to minimize radiated sound power and the radiation efficiency. The best design among the numerous feasible designs of a rectangular plate could be achieved. However, general insight seems more necessary to be helpful to a design engineer, even though such optimization delivered a good result.

Park et al. [10] investigated sound that radiated from the rectangular plate, based on the Rayleigh-Ritz method, where general boundary conditions can be taken into account. Sound radiation power is obtained based on the assumption that cross-modal terms disappear. Although this is only true for some particular conditions, the results demonstrate the corresponding approach is useful. It was shown that both velocity response of the plate and sound radiation are influenced by the edge conditions. However, detailed investigations related to different boundary conditions were not presented.

The present paper deals with sound radiated into the farfield of a rectangular plate, with different boundary conditions, pinned and guided. As discussed above, these two conditions seem mostly important in an investigation of general sound radiation characteristics, and furthermore, are greatly advantageous in numerical calculations. That is, as mentioned by Xie [8], using a pinned condition of the plate edges and an average over point force locations, the cross-modal terms become zero. The same approach can also be applied to the guided condition, except that in this case the so-called piston mode exists, which is an important phenomenon. Such an averaging approach seems useful to judge the general radiation characteristics in industries, rather than using the obtained information from the single point excitation, as studied by Berry [2].

General radiation characteristics, including radiation efficiency and radiation power, are studied. As the pinned case of a rectangular plate was already investigated by Xie [8], the guided condition is the focal point in the present paper. However, the pinned plate will be discussed if necessary. Different aspect ratios are also taken into account.

2. Radiation efficiency of a rectangular plate in a guided condition

2.1 Acoustic power radiated from a plate

Consider a rectangular plate as shown in Fig. 1, assumed that all edges are in guided conditions.

The velocity $v(\mathbf{x})$ at location $\mathbf{x}=(x,y)$ on the plate can be obtained by superposing the modal contributions from each mode.

$$v(\mathbf{x})=\sum_{m=0}^{\infty}\sum_{n=0}^{\infty}v_{mn}(\mathbf{x})=\sum_{m=0}^{\infty}\sum_{n=0}^{\infty}u_{mn}\psi_{mn}(\mathbf{x})=\sum_{m=0}\sum_{n=0}u_{mn}\psi_{mn}(\mathbf{x}) \quad (1)$$

where v_{mn} is the surface velocity distribution of the plate of mode (m,n), u_{mn} is the complex modal velocity amplitude, ψ_{mn} is the mode shape function of mode (m,n) and m, n are the indices of the modes. The mode shape function $\psi_{mn}(\mathbf{x})$ when all edges are in guided conditions is expressed as

$$\psi_{mn}(\mathbf{x})=\cos\left(\frac{m\pi x}{L_x}\right)\cos\left(\frac{n\pi y}{L_y}\right) \quad (2)$$

where L_x and L_y are the edge length in the corresponding co-ordinates x and y.

The complex acoustic pressure amplitude $p(\mathbf{r})$ at a location expressed in spherical co-ordinates $r=(r,\theta,\phi)$ at frequency ω can be written in terms of the plate surface velocity using Rayleigh integral [11]

$$p(\mathbf{r})=\frac{ik\rho c}{2\pi}\int_S v(\mathbf{x})\frac{e^{-ikr'}}{r'}d\mathbf{x} \quad (3)$$

where ρ, c are the air density and speed, $k=\omega/c$ is the acoustic wavenumber, S is the plate surface and the distance $r'=|\mathbf{r}-\mathbf{x}|$ as shown in Fig. 1.

Substituting Eq. (1) into Eq. (3) results in

$$p(\mathbf{r})=\sum_{m=0}\sum_{n=0}\frac{ik\rho c}{2\pi}\int_S u_{mn}\psi_{mn}(\mathbf{x})\frac{e^{-ikr'}}{r'}d\mathbf{x}=\sum_{m=0}\sum_{n=0}p_{mn} \quad (4)$$

For the farfield where $r >> L_x, L_y$ the effect of the difference in distance on the amplitude of the acoustic pressure can be ignored, while its effect on the phase remains important. Thus, the distance r' may be approximated as r [12].

$$r'=r-\sin\theta\cos\phi\cdot x/r-\sin\theta\sin\phi\cdot y/r \quad (5)$$

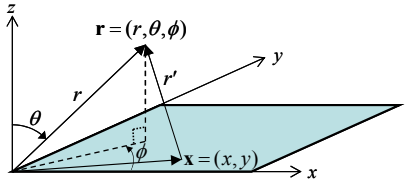

Fig. 1. Co-ordinate system of a vibrating rectangular plate.

Then, the complex acoustic pressure amplitude p_{mn} corresponding mode (*m*,*n*) in Eq. (4) can be written as, in the Cartesian co-ordinates [13]

$$p_{mn} = ik\rho c\frac{e^{-ikr}}{2\pi r}\int_0^b\int_0^a u_{mn}\psi_{mn}\times\exp\left[i\left(\alpha x/L_x\right)+i\left(\beta y/L_y\right)\right]dxdy \tag{6}$$

Substituting Eq. (2) into Eq. (6) and some algebraic manipulations [14] gives

$$p_{mn} = -ik\rho c\frac{e^{-ikr}}{2\pi r}u_{mn}\alpha\beta L_xL_y\left[\frac{(-1)^m\exp(i\alpha)-1}{m^2\pi^2-\alpha^2}\right]\left[\frac{(-1)^n\exp(i\beta)-1}{n^2\pi^2-\beta^2}\right] \tag{7}$$

Thus,

$$p(\mathbf{r}) = \sum_{m=0}\sum_{n=0}p_{mn} = \sum_{m=0}\sum_{n=0}u_{mn}A_{mn}(\mathbf{r}) \tag{8}$$

where

$$A_{mn}(\mathbf{r}) = -ik\rho c\frac{e^{-ikr}}{2\pi r}\alpha\beta L_xL_y\left[\frac{(-1)^m\exp(i\alpha)-1}{m^2\pi^2-\alpha^2}\right]\left[\frac{(-1)^n\exp(i\beta)-1}{n^2\pi^2-\beta^2}\right] \tag{9}$$

where $\alpha = kL_x\sin\theta\cos\phi$, $\beta = kL_y\sin\theta\sin\phi$ and $r = |\mathbf{r}|$.

The total acoustic power that is radiated from the plate can be obtained by integrating the farfield acoustic intensity over hemisphere of radius *r* to give

$$W = \int_0^{2\pi}\int_0^{\pi/2}\frac{|p(\mathbf{r})|^2}{2\rho c}r^2\sin\theta d\theta d\phi \tag{10}$$

Therefore, the total acoustic power can be expressed in terms of u_{mn} and $A_{mn}(\mathbf{r})$ from Eq. (8) as

$$\begin{aligned}W &= \int_0^{2\pi}\int_0^{\pi/2}\frac{p(\mathbf{r})p^*(\mathbf{r})}{2\rho c}r^2\sin\theta d\theta d\phi\\ &= \sum_{m=0}\sum_{n=0}\sum_{m'=0}\sum_{n'=0}u_{mn}u_{mn}^*\int_0^{2\pi}\int_0^{\pi/2}A_{mn}(\mathbf{r})A_{mn}^*(\mathbf{r})\frac{r^2}{2\rho c}\sin\theta d\theta d\phi\end{aligned} \tag{11}$$

This equation shows that the total acoustic power requires, in general, cross-modal terms and knowledge of the excitation, as modal velocities u_{mn}, u_{mn}^* seen in the equation.

2.2 Point force excitation

The complex modal velocity amplitude u_{mn} due to a point force applied at (x_e, y_e) on the plate is

$$u_{mn} = \frac{i\omega F\psi_{mn}(x_e,y_e)}{\left[\omega_{mn}^2(1+i\eta)-\omega^2\right]M_{mn}} \tag{12}$$

where F is the complex force amplitude, ω_{mn} is the natural frequency, η is the damping loss factor and M_{mn} is the modal mass, which is

$$\begin{aligned}M_{mn} &= \int_0^{Lx}\int_0^{Ly}\rho_p t\psi_{mn}^2(x,y)dxdy\\ &= \begin{cases}\rho_p tL_xL_y & \text{for } m=0 \text{ and } n=0\\ \rho_p tL_xL_y/2 & \text{for } m=0 \text{ or } n=0\\ \rho_p tL_xL_y/4 & \text{for } m\neq 0 \text{ and } n\neq 0\end{cases}\end{aligned} \tag{13}$$

where ρ_p and *t* are the density and thickness of the plate. The corresponding natural frequency ω_{mn} is given by

$$\omega_{mn}^2 = \left(\frac{D}{\rho_p t}\right)^{1/2}\left[\left(\frac{m\pi}{L_x}\right)^2+\left(\frac{n\pi}{L_y}\right)^2\right] \tag{14}$$

where D is the bending stiffness of the plate.

2.3 Average radiation efficiency to point force excitations

The general characteristics of the response are investigated by averaging them over the point force excitations. This shows advantages, as the cross-modal terms can be eliminated and thus, the calculation time can be greatly reduced.

The spatially and temporally averaged mean square velocity of the plate in mode (*m*,*n*) is found by [13]

$$\left\langle\overline{v_{mn}^2}\right\rangle = \begin{cases}|u_{mn}|^2/2 & \text{for } m=0 \text{ and } n=0\\ |u_{mn}|^2/4 & \text{for } m=0 \text{ or } n=0\\ |u_{mn}|^2/8 & \text{for } m\neq 0 \text{ and } n\neq 0\end{cases} \tag{15}$$

Similarly, the spatially averaged mean square velocity in mode (*m*,*n*), averaged over all possible force positions, i.e. averaged over both the forces and responses, can be found. For $m\neq 0$ and $n\neq 0$,

$$\begin{aligned}\left\langle\left\langle\overline{v_{mn}^2}\right\rangle\right\rangle_e &= \frac{1}{L_xL_y}\int_0^{Lx}\int_0^{Ly}\left\langle\overline{v_{mn}^2}\right\rangle dx_edy_e = \frac{1}{L_xL_y}\int_0^{Lx}\int_0^{Ly}\frac{|u_{mn}|^2}{8}dx_edy_e\\ &= \frac{1}{32}\frac{\omega^2|F|^2}{\left[(\omega_{mn}^2-\omega^2)^2+\eta^2\omega_{mn}^4\right]M_{mn}^2}\end{aligned} \tag{16}$$

The same mathematics can be applied for mode cases $(m=0 \text{ and } n=0)$ and $(m=0 \text{ or } n=0)$, and the results are summarized as

$$\left\langle\left\langle\overline{v_{mn}^2}\right\rangle\right\rangle_e = \begin{cases}\dfrac{1}{2}\dfrac{\omega^2|F|^2}{\left[(\omega_{mn}^2-\omega^2)^2+\eta^2\omega_{mn}^4\right]M_{mn}^2} & \text{for } m=0 \text{ and } n=0\\ \dfrac{1}{8}\dfrac{\omega^2|F|^2}{\left[(\omega_{mn}^2-\omega^2)^2+\eta^2\omega_{mn}^4\right]M_{mn}^2} & \text{for } m=0 \text{ or } n=0\\ \dfrac{1}{32}\dfrac{\omega^2|F|^2}{\left[(\omega_{mn}^2-\omega^2)^2+\eta^2\omega_{mn}^4\right]M_{mn}^2} & \text{for } m\neq 0 \text{ and } n\neq 0\end{cases} \tag{17}$$

Note that, here, modal mass M_{mn} is dependent on the number m and n. The spatially averaged mean square velocity, averaged over all possible force locations, is given by

$$\left\langle\left\langle \overline{v^2} \right\rangle\right\rangle_e = \sum_{m=0}\sum_{n=0}\left\langle\left\langle \overline{v_{mn}^2} \right\rangle\right\rangle_e \tag{18}$$

The sound power radiated from the plate that averaged over all possible point forces can be written. From Eq. (11),

$$\begin{aligned}\langle W\rangle_e &= \frac{1}{L_x L_y}\int_0^{Lx}\int_0^{Ly} W dx_e dy_e \\ &= \sum_{m=0}\sum_{n=0}\sum_{m'=0}\sum_{n'=0}\frac{1}{L_x L_y}\int_0^{Lx}\int_0^{Ly} u_{mn}u_{m'n'}^* dx_e dy_e \\ &\quad \int_0^{2\pi}\int_0^{\pi/2} A_{mn}(\mathbf{r})A_{m'n'}^*(\mathbf{r})\frac{r^2}{2\rho c}\sin\theta d\theta d\phi\end{aligned} \tag{19}$$

It should be noted that

$$\begin{aligned}&\sum_{m=0}\sum_{n=0}\sum_{m'=0}\sum_{n'=0}\frac{1}{L_x L_y}\int_0^{Lx}\int_0^{Ly} u_{mn}u_{m'n'}^* dx_e dy_e \\ &\qquad = \sum_{m=0}\sum_{n=0}\frac{1}{L_x L_y}\int_0^{Lx}\int_0^{Ly} u_{mn}u_{mn}^* dx_e dy_e\end{aligned} \tag{20}$$

as the orthogonality of the eigenfunctions holds. Thus, Eq. (19) can be simplified to

$$\begin{aligned}\langle W\rangle_e &= \sum_{m=0}\sum_{n=0}\frac{1}{L_x L_y}\int_0^{Lx}\int_0^{Ly} u_{mn}u_{mn}^* dx_e dy_e \\ &\quad \int_0^{2\pi}\int_0^{\pi/2} A_{mn}(\mathbf{r})A_{mn}^*(\mathbf{r})\frac{r^2}{2\rho c}\sin\theta d\theta d\phi \\ &= \sum_{m=0}\sum_{n=0} W_{mn}\end{aligned} \tag{21}$$

which shows that the cross-modal terms have been eliminated and the averaged sound power is the sum of the power radiated by each mode [8]

$$W_{mn} = \frac{1}{L_x L_y}\int_0^{Lx}\int_0^{Ly} u_{mn}u_{mn}^* dx_e dy_e \int_0^{2\pi}\int_0^{\pi/2} A_{mn}(\mathbf{r})A_{mn}^*(\mathbf{r})\frac{r^2}{2\rho c}\sin\theta d\theta d\phi \tag{22}$$

Substituting the relationship of $\left\langle\left\langle \overline{v_{mn}^2} \right\rangle\right\rangle$ and $|u_{mn}|^2$ shown in Eq. (16) into Eq. (22) gives the modal radiation efficiency, summarized as

$$\begin{aligned}\sigma_{mn} &= \frac{W_{mn}}{\rho c L_x L_y \left\langle\left\langle \overline{v_{mn}^2} \right\rangle\right\rangle_e} \\ &= \begin{cases} \dfrac{\int_0^{2\pi}\int_0^{\pi/2} A_{mn}(\mathbf{r})A_{mn}^*(\mathbf{r}) r^2\sin\theta d\theta d\phi}{\rho^2 c^2 L_x L_y} & \text{for } m=0 \text{ and } n=0 \\ \dfrac{2\int_0^{2\pi}\int_0^{\pi/2} A_{mn}(\mathbf{r})A_{mn}^*(\mathbf{r}) r^2\sin\theta d\theta d\phi}{\rho^2 c^2 L_x L_y} & \text{for } m=0 \text{ or } n=0 \\ \dfrac{4\int_0^{2\pi}\int_0^{\pi/2} A_{mn}(\mathbf{r})A_{mn}^*(\mathbf{r}) r^2\sin\theta d\theta d\phi}{\rho^2 c^2 L_x L_y} & \text{for } m\neq 0 \text{ and } n\neq 0 \end{cases}\end{aligned} \tag{23}$$

Substituting Eq. (9) into Eq. (23) and algebraic manipulations gives the simplified modal radiation efficiency. For $m \neq 0$ and $n \neq 0$, it is found as

$$\sigma_{mn} = 16\frac{k^2 L_x L_y}{\pi^2} \int_0^{2\pi}\int_0^{\pi/2}\alpha^2\beta^2 \frac{\sin^2\left(\frac{\alpha}{2}\right)\cos^2\left(\frac{\alpha}{2}\right)\sin^2\left(\frac{\beta}{2}\right)\cos^2\left(\frac{\beta}{2}\right)}{\left[\alpha^2-(m\pi)^2\right]^2\left[\beta^2-(n\pi)^2\right]^2}\sin\theta d\theta d\phi$$

For general mode cases, they can be summarized as

$$\sigma_{mn} = \begin{cases} 4\dfrac{k^2 L_x L_y}{\pi^2}\displaystyle\int_0^{2\pi}\int_0^{\pi/2}\frac{\sin^2\left(\frac{\alpha}{2}\right)\cos^2\left(\frac{\alpha}{2}\right)\sin^2\left(\frac{\beta}{2}\right)\cos^2\left(\frac{\beta}{2}\right)}{\left[\alpha-(m\pi)^2/\alpha\right]^2\left[\beta-(n\pi)^2/\beta\right]^2}\sin\theta d\theta d\phi \\ \qquad \text{for } m=0 \text{ and } n=0 \\ 8\dfrac{k^2 L_x L_y}{\pi^2}\displaystyle\int_0^{2\pi}\int_0^{\pi/2}\frac{\sin^2\left(\frac{\alpha}{2}\right)\cos^2\left(\frac{\alpha}{2}\right)\sin^2\left(\frac{\beta}{2}\right)\cos^2\left(\frac{\beta}{2}\right)}{\left[\alpha-(m\pi)^2/\alpha\right]^2\left[\beta-(n\pi)^2/\beta\right]^2}\sin\theta d\theta d\phi \\ \qquad \text{for } m=0 \text{ or } n=0 \\ 16\dfrac{k^2 L_x L_y}{\pi^2}\displaystyle\int_0^{2\pi}\int_0^{\pi/2}\frac{\sin^2\left(\frac{\alpha}{2}\right)\cos^2\left(\frac{\alpha}{2}\right)\sin^2\left(\frac{\beta}{2}\right)\cos^2\left(\frac{\beta}{2}\right)}{\left[\alpha-(m\pi)^2/\alpha\right]^2\left[\beta-(n\pi)^2/\beta\right]^2}\sin\theta d\theta d\phi \\ \qquad \text{for } m\neq 0 \text{ and } n\neq 0 \end{cases} \tag{24}$$

Note that $\cos^2$ is used when m or n is an odd integer and $\sin^2$ is used when m or n is an even integer.

The similar expression of the modal radiation efficiency for the pinned plate in an infinite baffle is already shown by [8], as

$$\sigma_{mn} = \frac{64k^2 L_x L_y}{\pi^6 m^2 n^2}\int_0^{\pi/2}\int_0^{\pi/2}\frac{\sin^2\left(\frac{\alpha}{2}\right)\cos^2\left(\frac{\alpha}{2}\right)\sin^2\left(\frac{\beta}{2}\right)\cos^2\left(\frac{\beta}{2}\right)}{\left[(\alpha/(m\pi))^2-1\right]^2\left[(\beta/(n\pi))^2-1\right]^2}\sin\theta d\theta d\phi \tag{25}$$

Finally, the average radiation efficiency, over all possible point force positions, can be obtained for the total radiated power in terms of a summation of modal radiated power.

$$\begin{aligned}\sigma &= \frac{\sum_{m=0}\sum_{n=0} W_{mn}}{\rho c L_x L_y \sum_{m=0}\sum_{n=0}\left\langle\left\langle \overline{v_{mn}^2} \right\rangle\right\rangle_e} = \frac{\sum_{m=0}\sum_{n=0}\sigma_{mn}\left\langle\left\langle \overline{v_{mn}^2} \right\rangle\right\rangle_e}{\sum_{m=0}\sum_{n=0}\left\langle\left\langle \overline{v_{mn}^2} \right\rangle\right\rangle_e} \\ &= \frac{\sum_{m=0}\sum_{n=0}\sigma_{mn}\left[(\omega_{mn}^2-\omega^2)^2+\eta^2\omega_{mn}^4\right]^{-1}M_{mn}^{-2}}{\sum_{m=0}\sum_{n=0}\left[(\omega_{mn}^2-\omega^2)^2+\eta^2\omega_{mn}^4\right]^{-1}M_{mn}^{-2}}\end{aligned} \tag{26}$$

3. Numerical investigation

3.1 Rectangular plate

The dimensions and material properties of the steel plate are the same as those used in Berry [2] (Table 1). The fundamen-

Table 1. Material properties and dimensions of the baseline model shown in Fig. 1.

Young's modulus, E (GNm^{-2})	199.	Plate length, L_x (m)	0.455
Poisson's ratio, ν	0.28	Plate width, L_y (m)	0.455/1.2
Density, ρ_p (kgm^{-3})	7850.0	Plate thickness, t (mm)	1.0
DLF of the plate, η	0.1	Air speed (ms^{-1})	343.

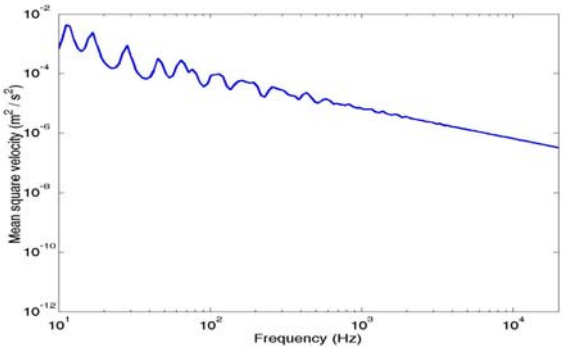

Fig. 2. Average velocity of a rectangular plate.

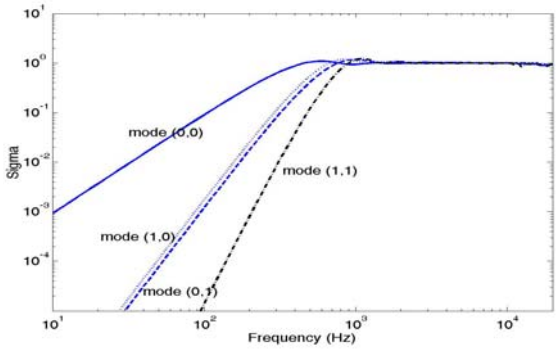

Fig. 3. Modal radiation efficiency of a rectangular plate.

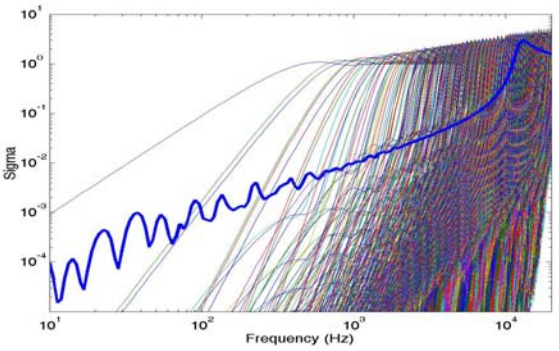

Fig. 4. Modal and average radiation efficiency of a rectangular plate with guided edges.

tal mode (1,1) is found at 28.0 Hz and the critical frequency is 12365 Hz (maximum frequency of 20 kHz and 40 frequency points per logarithmic frequency decade are used). A unit point force is used in the calculation.

Firstly, the spatially averaged mean square velocity, averaged over all possible force locations (Eq. (18)), is shown in Fig. 2, where no dominant peaks are found at mid- and high frequencies.

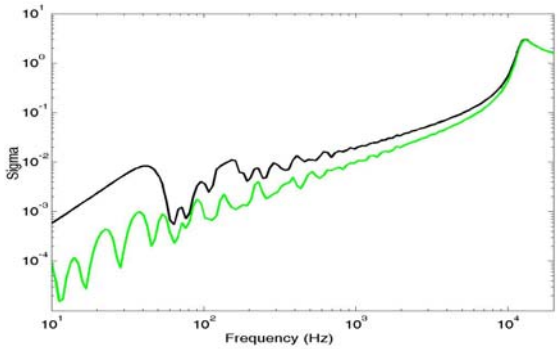

Fig. 5. Average radiation efficiency of a rectangular plate with pinned edges (black) and guided edges (grey).

To verify if the numerical calculation is appropriate, the modal radiation efficiencies (Eq. (24)) of first 4 modes are plotted in Fig. 3. Then the so-called piston mode (mode (0,0)) is the most efficient in radiation and it can be seen that all results agree well with those presented in Berry [2].

The modal radiation efficiencies of all modes and the average (Eq. (26)) are shown together in Fig. 4. Also, the average radiation efficiency is compared to that of the pinned plate investigated by Xie [8], in Fig. 5. For comparison, the same dimensions for both cases are used. It can be seen that the physical phenomenon is dependent on boundary conditions. The dominant peak, near the fundamental frequency of mode (1,1), shown from the pinned plate, cannot be found in the guided case and therefore, there is no clear low frequency limit of so-called corner and edge mode regions. At low frequencies, the average radiation efficiency of the pinned plate is higher than that of the guided, even though no rigid mode occurs in the pinned plate. Meanwhile, it becomes maximum at the critical frequency, regardless of boundary conditions.

As previously studied for the pinned plate, for example, in Xie [8], it is the corner and edge mode region that is strongly dependent on structural damping. The damping effect for the guided plate is investigated. Fig. 6(a) shows how the average radiation efficiency of the guided plate changes when the damping of the plate varies. (Note that only the low frequency region is shown.) The radiation efficiency is strongly dependent on the damping, at lower frequencies, as well as at higher frequencies of the fundamental frequency. In contrast, it can be seen that, for the pinned plate, there are no changes below the fundamental frequency (Fig. 6(b)). For both cases, increasing damping results in more efficient radiation. This is because vibrational velocity of the plate will substantially reduce [8].

In addition to radiation efficiency, it seems important to examine radiation power, where structural response of the plate is due to excitation being taken into account. In Fig. 7, the average radiation powers are compared for the two boundary conditions. Similar to the radiation efficiency, it can be seen that the power radiated by the pinned plate is higher than that

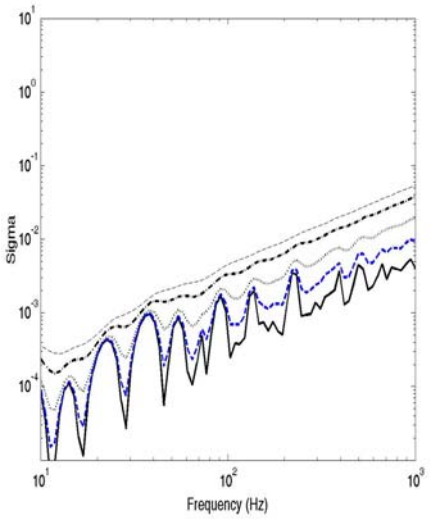

(a)

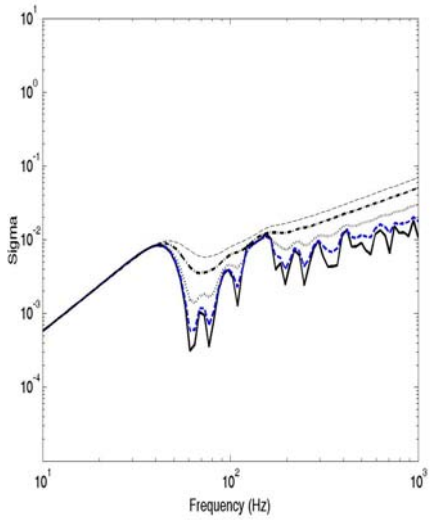

(b)

Fig. 6. Average radiation efficiency of a rectangular plate with guided edges (left) and with pinned edges (right). ——— , η =0.05; - - - , η =0.1; ····· , η =0.2; -·-·- , η =0.4; – – – , η =0.6.

by the guided below the critical frequency. While radiation due to the fundamental frequency mode is clearly visible for the pinned plate, it is difficult to find any particular peak related to the motion of the guided plate below the critical frequency. It seems that the power level is generally governed by the piston mode of the guided plate. For comparison, the power radiated only from the piston mode is also shown in the same figure (dotted line), found by [2].

$$W = \rho\ /(4\pi c\rho_p{}^2 t^2) \tag{27}$$

3.2 Strip plate

It is already known that radiation characteristics depend on the aspect ratio of a plate [8, 13]. In this section, the aspect ratio of 12.0 is considered, where only L_y is changed (the previous section dealt with the aspect ratio of 1.2).

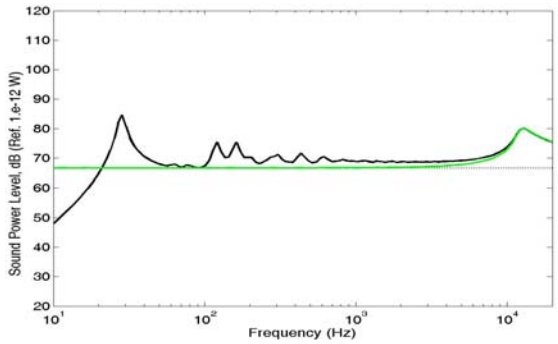

Fig. 7. Acoustic power radiated from a rectangular plate with pinned edges (black) and guided edges (grey); averaged for both response and excitation.

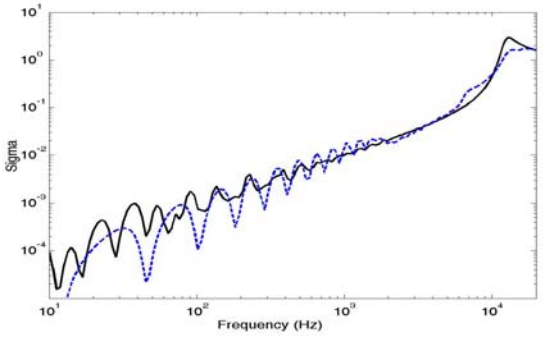

Fig. 8. Average radiation efficiency of a plate (solid, aspect ratio of 1.2) and a strip (dashed, aspect ratio of 12.0) with guided edges; averaged for both response and excitation.

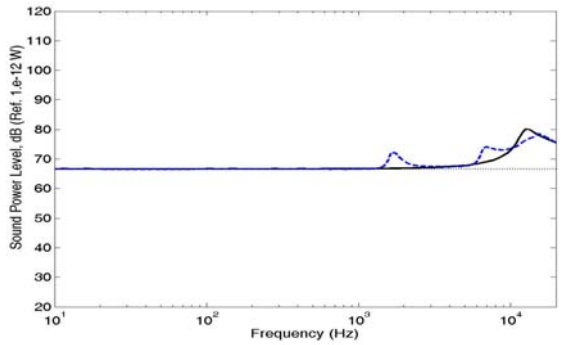

Fig. 9. Acoustic power radiated from a plate (solid, aspect ratio of 1.2) and a strip (dashed, aspect ratio of 12.0) with guided edges; averaged for both response and excitation.

The average radiation efficiency and average radiation power of the guided plate are respectively compared in Figs. 8 and 9, where it can be seen how they change for different aspect ratios. The radiation efficiency of the strip reduces at the critical frequency. The acoustic power increases at frequencies of modes (m,n) = $(0,n)$ (i.e. 1655, 6620, 14890 Hz), which means the radiation is maximised where the wavelength is $n\times L_y$ of the strip. This is because the vibrational level increases at these modes. Distinguishable are the three vibrational peaks that are found at high frequencies for the strip plate (the corresponding result is shown later at Fig. 12. Also

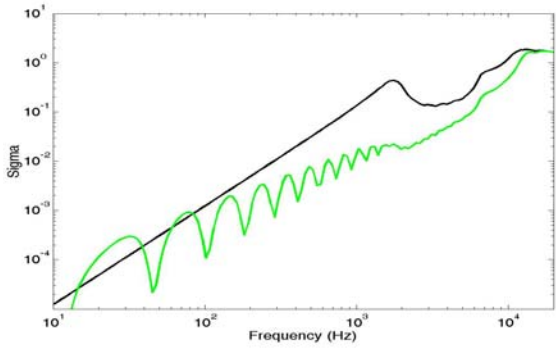

Fig. 10. Average radiation efficiency of a strip with pinned edges (black) and guided edges (grey); averaged for both response and excitation.

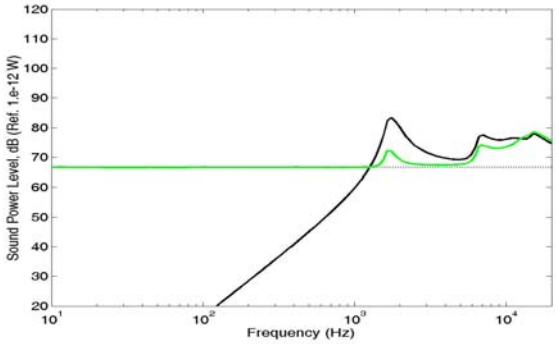

Fig. 11. Acoustic power radiated from a strip with pinned edges (black) and guided edges (grey); averaged for both response and excitation.

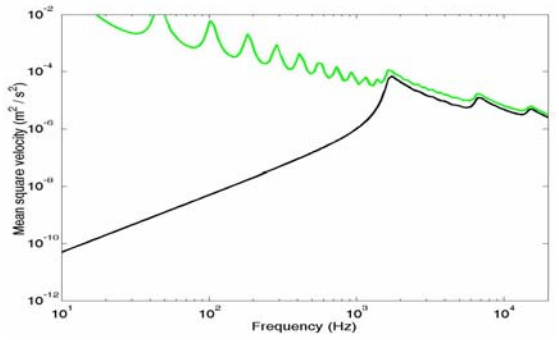

Fig. 12. Average velocity of a strip with pinned edges (black) and guided edges (grey).

notable is that the average velocity shown in Fig. 2 gives no particular peaks.)

The average radiation efficiency and average radiation power of the strip are respectively compared in Figs. 10 and 11, where it can be seen how they change for different boundary conditions. Recalling the results shown in Fig. 9, it is interesting that the radiation power becomes closer when above the frequency of mode $(m,n) = (0,1)$. It can be seen that radiation is maximised at the frequencies of modes $(m,n) = (0,1)$, (0,2), (0,3) (guided case) and at frequencies of mode $(m,n) = (1,1)$, (1,2), (1,3) (pinned case). As seen in Fig. 12, this is because the vibrational level increases at these frequencies, regardless of the boundary conditions considered in this study (the frequencies of the modes are very close. For example, 1655 Hz of guided mode (0,1) and 1666 Hz of pinned mode (1,1).) Radiation power at these frequencies seems greater than that radiated at the critical frequency. Below the frequency of mode $(m,n) = (0,1)$, radiation due to the rigid mode of the guided plate, is greater than radiation from the pinned.

4. Concluding remarks

The modal radiation efficiency and average radiation efficiency for possible point excitation locations are analytically investigated for the plate whose edges are in guided conditions. In such boundary conditions, it is possible to eliminate the cross-modal term in obtaining the average quantities. The numerical calculation and comparison of the acoust ic characteristics, with those of the plate with pinned conditions, can cause some physical phenomena to be found and be summarized as follows.

While the pinned plate shows acoustic characteristics at fundamental and critical frequencies and the so-called corner and edge mode frequencies, for the guided plate with moderate aspect ratio, only the critical frequency seems related to the radiation efficiency at high frequencies. Below that frequency, it was found that the so-called piston mode (rigid mode) dominates acoustic radiation. This is consistent with the result when a single point is excited, as discussed by Berry [2].

It is known that the radiation efficiency of the pinned plate increases at the corner and edge mode regions if the plate damping increases, as the vibrational level decreases. For the guided case, the same phenomenon is found below the critical frequency. However, the impact due to this is, in fact, very small as the radiation is dominated by the piston mode.

For the strip with large aspect ratio, radiation is related to the mode of the short edges. That is, radiation power is maxima where the y-directional wavelength is n (= 1, 2, 3, ⋯) times L_y. This is because the vibrational level of the strip (with the guided as well as the pinned), at these mode frequencies, shows clear difference.

As Berry identified [2], a piston mode is mostly important in the acoustic radiation at low frequencies, for both the guided and free conditions. Also, Lomas and Hayek [5] pointed out that the radiation powers of the pinned and clamped plates are at a similar level. In addition to these studies, the present study on the characteristics of the guided plate, which is compared to the pinned case, may provide insight to predict general characteristics of acoustic radiation.

References

[1] K.-S. Chae, J.-H. Jeong, C.-M. Park and J. W. Yoo, Prediction and Improvement of High-Frequency Road Noise of a Mid-Size Sedan, SAE., 2007-01-2307.

[2] A. Berry, J.-L. Guyader and J. Nicolas, A general formula-

tion for the sound radiation from rectangular, baffled plates with arbitrary boundary conditions, *J. Acoust. Soc. Am.*, 88 (1990) 2792-2802.

[3] G. Maidanik, Response of ribbed panels to reverberant acoustic fields, *J. Acoust. Soc. Am.*, 34 (1962) 809-826.

[4] F. G. Leppington, E. G. Broadbent and K. H. Heron, The acoustic radiation efficiency of rectangular panels, *Proc. the Royal Society London A*, 382 (1982) 245-271.

[5] N. S. Lomas and S. I. Hayek, Vibration and acoustic radiation of elastically supported rectangular plates, *Journal of Sound and Vibration*, 52 (1977) 1-25.

[6] S. Snyder and N. Tanaka, Calculating total acoustic power output using modal radiation efficiencies, *J. Acoust. Soc. Am.*, 97 (1995) 1702-1709.

[7] W. L. Li and H. J. Gibeling, Acoustic radiation from a rectangular plate reinforced by finite springs at arbitrary locations, *Journal of Sound and Vibration*, 220 (1990) 117-133.

[8] G. Xie, D. J. Thompson and C. J. C. Jones, The radiation efficiency of baffled plates and strips, *Journal of Sound and Vibration*, 280 (2005) 181-209.

[9] A. R. Patil and M. J. Crocker, Prediction and Optimization of radiated sound power and radiation efficiency of vibrating structures using FEM, SAE 2000-01-0726.

[10] J. Park, L. Mongeau and T. Siegmund, Influence of support properties on the sound radiated from the vibrations of rectangular plate, *Journal of Sound and Vibration*, 264 (2003) 775-794.

[11] L. Rayleigh, *The Theory of Sound,* 2nd Edition, (1896) (reprinted by Dover, New York, 1945).

[12] L. Shuyu, Study on the radiation acoustic field of rectangular radiators in flexural vibration, *Journal of Sound and Vibration*, 254 (2002) 469-479.

[13] C. E. Wallace, Radiation resistance of a rectangular panel, *J. Acoust. Soc. Am.*, 51 (1972) 946-952.

[14] *Standard Mathematical Tables*, CRC Press, (1984).

Ji Woo Yoo received his BS and MS degrees in Precision Mechanical Engineering from Hanyang University, Seoul, in 1993 and 1995, respectively. He then studied in the ISVR, Southampton University, United Kingdom, where he received his PhD degree, in 2005. He currently works in CAE Tech Team, Hyundai Motor Company. His research interests are vibro-acoustics, hybrid approaches combining numerical methods, and mid- and high frequency problems of automotive vehicles.